solids

MDPI

Article

The Effect of the Formation of Superelastic NiTi Phase on Static and Dynamic Corrosion Performance of Ni-P Coating

Zhi Li * and Zoheir Farhat

Department of Mechanical Engineering, Dalhousie University, Halifax, NS B3J 2X4, Canada; Zoheir.Farhat@dal.ca
* Correspondence: Zhi.Li@dal.ca

Abstract: The addition of superelastic NiTi particles is a great benefit to the toughness of the Ni-P coating. Nonetheless, NiTi nanopowder costs 10 times more than Ti nanopowder. Therefore, in the present study, to reduce the cost, Ni-P-NiTi composite coatings were prepared on AISI 1018 steel substrates by the electroless incorporation of Ti nanoparticles into Ni-P followed by the annealing of Ni-P-Ti coatings. The effect of the formation of a superelastic NiTi phase on static and dynamic corrosion performance was investigated. It was found that the annealed Ni-P-Ti coating (i.e., Ni-P-NiTi coating) has much higher static corrosion resistance than the as-deposited Ni-P coating. The dynamic corrosion rates in the absence of abrasive particles are 10 times higher than the static corrosion rates of the coatings. The dynamic corrosion rates in the presence of abrasive particles are one order of magnitude higher than the dynamic corrosion rates in the absence of abrasive particles. The formation of a superelastic NiTi phase considerably improved the static and dynamic corrosion performance of the Ni-P coating. In the absence of abrasive particles under flowing condition, the dynamic corrosion resistance of the annealed Ni-P-Ti coating (i.e., Ni-P-NiTi coating) is 19 times higher than that of the as-deposited Ni-P coating. In the most aggressive environment (in the presence of abrasive particles), the dynamic corrosion resistance of the annealed Ni-P-Ti coating (i.e., Ni-P-NiTi coating) is four times higher than that of the as-deposited Ni-P coating. The annealed Ni-P-Ti coating (i.e., Ni-P-NiTi coating) can be used in applications where high corrosion resistance is required, especially in an extremely aggressive environment.

Keywords: Ni-P-NiTi composite coating; superelastic NiTi; static corrosion; dynamic corrosion

Citation: Li, Z.; Farhat, Z. The Effect of the Formation of Superelastic NiTi Phase on Static and Dynamic Corrosion Performance of Ni-P Coating. *Solids* **2021**, *2*, 278–292. https://doi.org/10.3390/solids2030018

Academic Editor: Francisco J. G. Silva

Received: 9 May 2021
Accepted: 28 July 2021
Published: 2 August 2021

1. Introduction

Low-carbon steels have been extensively used in construction, automotive, and the oil and gas industries due to their low cost and wide availability [1]. However, the corrosion resistance of low-carbon steels is inadequate to withstand a corrosive environment. For example, in the oil and gas industry, material degradation caused by corrosion is a severe problem especially in the presence of abrasive particles (i.e., sands or other solid particulates) [2]. For instance, the impacts of abrasive particles produce a strained surface that is highly vulnerable to corrosion due to the high energy of the surface [3]. Furthermore, under static condition, an oxide passive layer is formed on the surface, which prevents the steels from further corrosion [4]. In the presence of abrasive particles, the impacts of abrasive particles remove the oxide layer and expose a vulnerable fresh surface to the corrosive environment [5]. Due to these factors, the presence of abrasive particles significantly accelerates corrosion rate. To protect the steels from corrosion, various coatings have been developed. However, each of those coatings has their limitations. In addition to their low hardness, polymer-based coatings cannot withstand thermal and impact damage during assembly and operation processes [6], and epoxy-based coatings are not capable of resisting certain chemicals in crude oil, especially in the presence of abrasive particles [7]. Therefore, it is necessary to develop a protective coating that provides the highest protection to the steels against the corrosive environment.

Electroless Ni-P has been utilized in some industries as a protective coating owing to its high hardness and good corrosion resistance [8–10]. Therefore, an electroless Ni-P coating is a potential material to protect low-carbon steels from corrosion. However, the electroless Ni-P coating tends to readily crack under load or during impact due to its low toughness [11]. One way to improve the toughness of Ni-P coating is by the addition of nano-size superelastic NiTi particles. NiTi alloy is known for its high toughness and impact resistance [12]. Nevertheless, the high price of superelastic NiTi powder restricts its application. Since the price of nano-size Ti powder is 10 times lower than that of NiTi powder, Ti nano powder is a more attractive alternative. Therefore, in the present study, to reduce the cost, Ni-P-NiTi composite coatings were prepared by incorporating Ti nanoparticles into the Ni-P matrix followed by the annealing of Ni-P-Ti coatings. The formation of superelastic NiTi phase after annealing considerably improved the toughness of Ni-P coating, as confirmed in our previous study [13]. In addition, the adhesion between the coating and the steel substrate was also improved, as verified in another study [14]. However, the corrosion resistance of Ni-P-NiTi coatings has not been comprehensively studied.

There are still some disagreements on the effect of particles addition on the static corrosion resistance of Ni-P coatings in still 3.5 wt % sodium chloride solutions. Some researchers found that the addition of particles could improve the corrosion performance of Ni-P coatings. For example, Zahra et al. found that the incorporation of ZnO particles into Ni-P matrix improved the corrosion resistance of Ni-P coating in a still 3.5 wt % sodium chloride solution [15]. Ghavidel et al. also reported that the addition of SiC particles is of great benefit to corrosion resistance of Ni-P coating [16]. On the other hand, other researchers reported that the incorporation of particles undermined the corrosion resistance of Ni-P coating. For instance, Li et al. reported that the addition of Al_2O_3 particles weakened the corrosion performance of Ni-P coating [17]. In addition, Dhakal et al. found that Ni-P-TaC coating exhibited a higher corrosion rate than Ni-P coating [18]. Therefore, it is still of great interest to investigate the static corrosion performance and mechanisms of Ni-P based composite coatings. The corrosion resistance of a protective surface coating plays a crucial role during operation, especially in an extremely aggressive environment (in the presence of corrosive species and abrasive particles). High strain surface caused by impacts of abrasive particles is more susceptible to the corrosive environment [19]. Additionally, cracking and fracture during impact may reduce the lifetime of the protective coatings and expose the vulnerable steel substrate to the corrosive environment [20]. Protective coatings may have high corrosion resistance in a still corrosive solution, while they may not be able to resist a dynamic corrosive solution, especially in the presence of abrasive particles in the solution. Sun et al. reported that the corrosion rate was significantly increased by the single particle erosion [21]. To the best of the author's knowledge, the dynamic corrosion performance (in the absence and presence of abrasive particles under flowing condition) of Ni-P-NiTi coatings has not been previously studied.

The main objective is to investigate the effect of the formation of superelastic NiTi particles on the static and dynamic corrosion performance of Ni-P coating. Static corrosion tests were performed on as-deposited and annealed Ni-P and Ni-P-Ti coatings in a still sodium chloride solution. Dynamic corrosion tests (in the absence and presence of abrasive particles) were conducted in a sodium chloride solution under flowing condition. The performance of as-deposited and annealed Ni-P and Ni-P-Ti coatings under static and dynamic corrosion conditions was compared. The corrosion mechanisms under different conditions were investigated.

2. Materials and Methods

2.1. Coating Preparation

AISI 1018 steel coupons (18 mm × 10 mm × 6 mm) were employed as substrates. Prior to electroless plating, the steel substrates were pretreated to acquire good surface finish and remove oxide layer, grease, and debris. Grinding, polishing, alkali, and acid solutions clean were implemented on the substrates in sequence. The grinding was carried

out using four different grit silicon carbide papers (240, 320, 400, and 600). The polishing was performed using three different sizes of diamond polishing solutions (9 μm, 3 μm, and 1 μm). Then, polished substrates were submerged in a heated alkali solution at 85 °C for 5 min. The alkali solution consists of 30 g/L sodium phosphate, 50 g/L sodium carbonate, and 30 g/L sodium hydroxide. Then, the alkali cleaned substrates were immersed in a 20 vol% sulfuric acid solution for 15 s. Between each pre-treatment step, the substrates were thoroughly rinsed using distilled water.

Electroless plating solutions were made from two commercial chemical solutions. One comprises 20 wt % $NiSO_4$ as a nickel source, and the other consists of 25 wt % $NaPO_2H_2$ as a reducing agent. Then, 1 g of Ti powder was added into a 1 L plating solution. The spherical Ti particles exhibit a bimodal particle size distribution. One major size is approximately 50 nm; the other is approximately 5 μm [22]. The temperature and pH of the plating solutions were monitored using a thermometer and a pH meter and maintained at 88 ± 2 °C and 4.7 ± 0.1, respectively. During electroless plating, to keep Ti particles suspended in the solution, a magnetic stirring (5 s^{-1}) was applied. The plating time depends on the coating thickness (approximately 50 μm), which ranged from 4 to 6 h [13]. Ni-P and Ni-P-Ti coatings were annealed in a vacuum furnace (1×10^{-5} Torr) at 650 °C for 2 h. The nominal heating and cooling rates were set to 20 °C/min.

2.2. Static Corrosion Test

Static corrosion tests were conducted on as-deposited and annealed coatings in a 3.5 wt % sodium chloride solution at room temperature using the potentiodyanmic polarization (PP) technique. The PP tests were performed using a PAR 273A potentiostat controlled by a Scribner software, CorrWare. A three-electrode cell was utilized consisting of a coated sample as a working electrode, a saturated calomel electrode (SCE) as a reference electrode, and a platinum (net shape) as a counter electrode. Then, 1 cm^2 of the coated surface was exposed to the electrolyte. Prior to each PP test, the samples were maintained in an open circuit state for 2 h to obtain a steady state. In the case of PP tests, a potential range from −0.25 to +0.25 V vs. the open circuit potential was employed with a scan rate of 0.167 mV/s. PP tests were performed on three samples to confirm the repeatability and reproducibility. The testing results were averaged, and the standard deviations were used as error bars. The surfaces of samples before and after static corrosion tests were examined using scanning electron microscope (SEM). The accelerating voltage and current for SEM were 15 kV and 15 μA, respectively.

2.3. Dynamic Corrosion Test

Dynamic corrosion tests were performed in a slurry pot corrosion tester. Figure 1 shows a schematic of the slurry pot corrosion tester. The tester consists of a 4 L glass vessel, a neoprene-lined impeller, and a three-electrode cell. The impeller is driven by a motor to impel the slurry against the sample surface. The other faces of the specimen were covered with epoxy except for the testing surface. Then, the covered specimen was mounted in the sample holder for dynamic corrosion tests. The uncovered surface area of 1.8 cm^2 was exposed to abrasive slurry. The abrasive slurry consists of 35 wt % AFS 50–70 silica sand and 3.5 wt % sodium chloride solution. The mean size of the abrasive particles ranges from 200 to 300 μm [23]. The normal impact velocity during the test is 0.26–2.21 m/s at an impeller speed of 900 rpm [24]. The potentiodyanmic polarization technique was employed to conduct dynamic corrosion tests in the absence of abrasive particles and in the presence of abrasive particles under flowing condition (900 rpm) in a 3.5 wt % sodium chloride solution. Prior to each PP test, the samples were maintained in an open circuit state for 2 h to obtain a steady state in the still abrasive solution. The three-electrode cell connected to a Gamry PC4/750 potentiostat allows for electrochemical tests, which includes a platinum (plate shape) as a counter electrode, a sample as a working electrode, and a saturated calomel electrode (SCE) as a reference electrode. A potential range from −0.25 to +0.25 V vs. the open circuit potential was employed with a scan rate of 0.167 mV/s. The dynamic

corrosion tests were repeated twice to confirm the repeatability and reproducibility. The testing results were averaged, and the standard deviations were employed as error bars. After dynamic corrosion tests, the surfaces of tested samples were examined using SEM. The accelerating voltage and current for SEM were 15 kV and 15 μA, respectively.

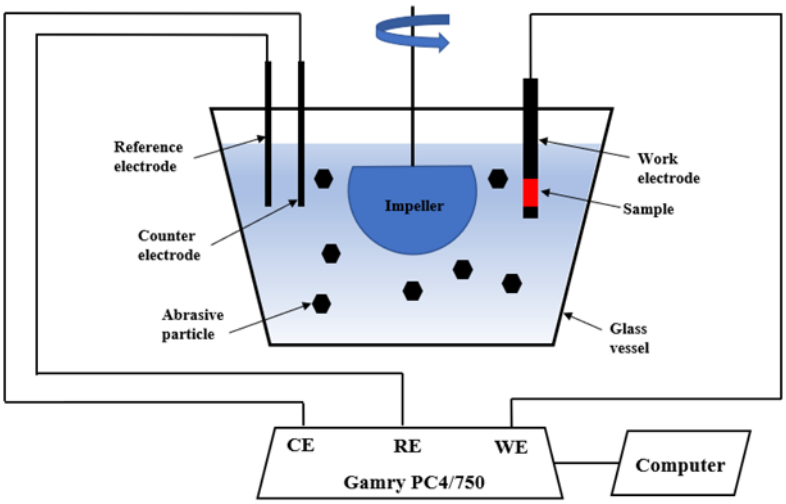

Figure 1. Schematic of slurry pot corrosion tester.

3. Results and Discussion

3.1. Coating Characterization

The corresponding Ti content in composite coating for 1g/L Ti powder in electroless plating solution is 5.1 wt % [13]. The XRD results of as-deposited Ni-P and 5.1 wt % Ti coatings have been discussed in our previous study [25]. As-deposited Ni-P and 5.1 wt % Ti coatings both exhibited amorphous Ni peaks, and the as-deposited 5.1 wt % Ti coating also contained low-intensity Ti XRD peaks [25]. In another study [13], we reported the XRD results of annealed Ni-P and 5.1 wt % Ti coatings. Highly preferred (200) orientation is observed in the XRD patterns of annealed Ni-P coating [13]. The formation of austenite NiTi phase in the annealed 5.1 wt % Ti coating is verified by slow scan XRD as well as point and line scan EDS [13]. Furthermore, the superelastic effect of NiTi phase in the annealed 5.1 wt % Ti coating is confirmed by nanoindentation tests [26]. Hence, in the rest of the manuscript, the as-deposited 5.1 wt % Ti coating is referred to as as-deposited Ni-P-Ti coating. After annealing, annealed 5.1 wt % Ti coating is referred to as annealed Ni-P-Ti coating (i.e., Ni-P-NiTi coating).

3.2. Static Corrosion Behavior

Static corrosion tests were conducted on as-deposited and annealed coatings in a still 3.5 wt % sodium chloride solution. The representative potentiodynamic polarization curves of AISI 1018 steel substrate, as-deposited, and annealed coatings are shown in Figure 2. Compared to AISI 1018 steel substrate, as-deposited and annealed coatings have much higher potential. This indicates that the as-deposited and annealed coatings have a lower corrosion tendency than the steel substrate.

The corrosion current density (i_{corr}) and corrosion potential (E_{corr}) were extracted from polarization curves (Figure 2) using Tafel extrapolation. Corrosion characteristics of AISI 1018 steel substrate, as-deposited, and annealed coatings are given in Table 1. The corrosion current of as-deposited Ni-P coating is one order of magnitude lower than AISI 1018 steel due to its amorphous microstructure and the formation of a passive NiO layer [25,27]. Compared to the as-deposited Ni-P coating, the as-deposited Ni-P-Ti coating exhibits much lower corrosion current, which is only one-third that of the as-deposited Ni-P coating. A similar trend is observed on annealed coatings; the corrosion current of an annealed Ni-P-Ti

coating is only one-third that of the annealed Ni-P coating. Furthermore, the corrosion currents of annealed coatings are slightly higher than those of as-deposited coatings.

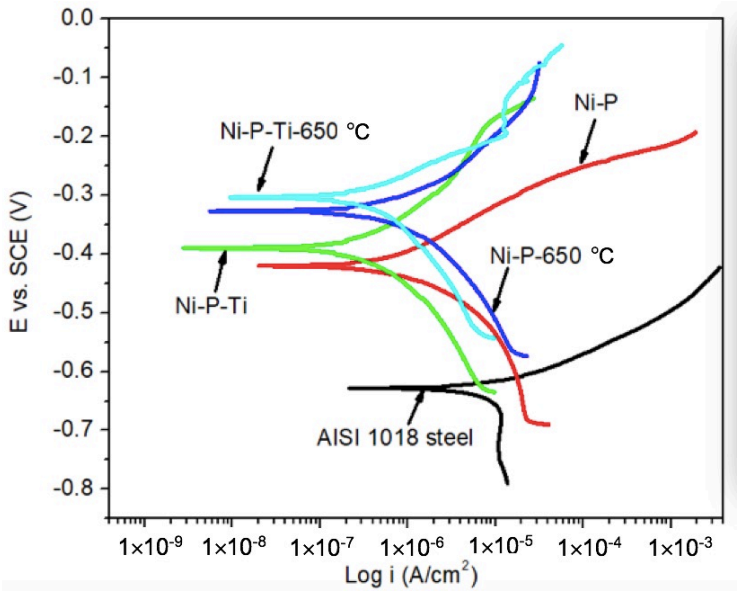

Figure 2. Representative potentiodynamic polarization curves of AISI 1018 steel substrate, as-deposited and annealed coatings in a still 3.5 wt % sodium chloride solution.

Table 1. Corrosion characteristics of AISI 1018 steel substrate, as-deposited coatings, and annealed coatings derived from polarization curves in static corrosion.

Samples	E_{corr} (V)	i_{corr} (μA/cm^2)
AISI 1018 steel	−0.627 ± 0.022	15.55 ± 1.50
Ni-P	−0.417 ± 0.025	1.07 ± 0.13
Ni-P-Ti	−0.389 ± 0.012	0.33 ± 0.10
Ni-P-650 °C	−0.327 ± 0.023	1.32 ± 0.14
Ni-P-Ti-650 °C	−0.304 ± 0.013	0.41 ± 0.13

3.3. Dynamic Corrosion in the Absence of Abrasive Particles

Dynamic corrosion tests in the absence of abrasive particles were performed in a 3.5 wt % sodium chloride solution under a flowing condition (900 rpm) up to 2 h. Figure 3 shows the representative potentiodynamic polarization curves of AISI 1018 steel substrate, as-deposited coatings, and annealed coatings in the absence of abrasive particles under a flowing condition (900 rpm). It is observed that the as-deposited and annealed coatings display much higher corrosion potential than the steel substrate. This suggests the lower corrosion tendency of the coatings than that of the steel substrate.

The corrosion current density (i_{corr}) and corrosion potential (E_{corr}) were extracted from polarization curves (Figure 3) using Tafel extrapolation. Dynamic corrosion characteristics of AISI 1018 steel substrate, as-deposited coatings, and annealed coatings in the absence of abrasive particles under a flowing condition (900 rpm) are given in Table 2. Compared to static corrosion (Table 1), the dynamic corrosion currents are much higher. For example, for as-deposited Ni-P coatings, the average dynamic corrosion current is 33.5 μA/cm^2, which is 33 times that of the static corrosion current (Table 1: 1.07 μA/cm^2). The as-deposited Ni-P-Ti coating exhibits a lower dynamic corrosion current than the as-deposited Ni-P coating. Similar to as-deposited coatings, the dynamic corrosion current of the annealed Ni-P-Ti coating is lower than that of the annealed Ni-P coating. The annealed Ni-P-Ti coating displays the lowest dynamic corrosion current (1.8 μA/cm^2) among all the tested coatings, which is only 5% of the dynamic corrosion current of the as-deposited Ni-P coating (33.5 μA/cm^2).

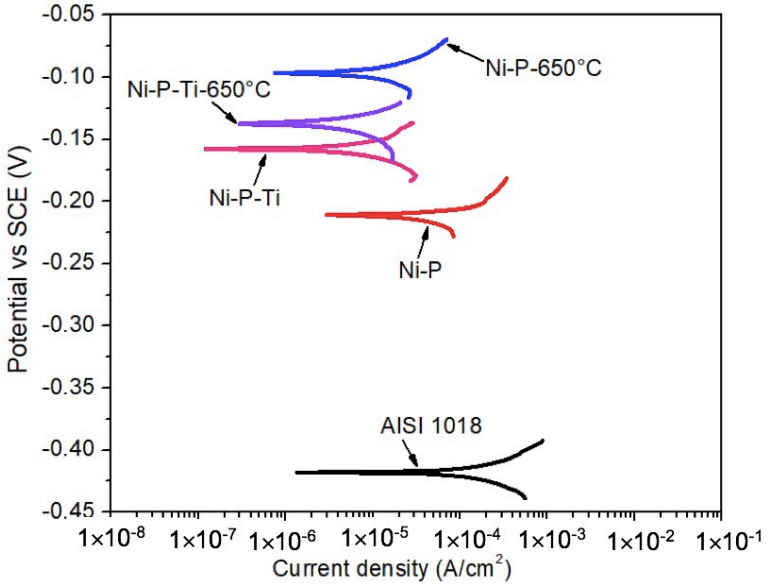

Figure 3. Representative potentiodynamic polarization curves of AISI 1018 steel substrate, as-deposited coatings, and annealed coatings in the absence of abrasive particles under a flowing condition (900 rpm).

Table 2. Corrosion characteristics of AISI 1018 steel substrate, as-deposited and annealed coatings derived from polarization curves in the absence of abrasive particles under a flowing condition (900 rpm).

Samples	E_{corr} (V)	i_{corr} (μA/cm^2)
AISI 1018 steel	−0.416 ± 0.005	91.1 ± 0.7
Ni-P	−0.218 ± 0.004	33.5 ± 0.5
Ni-P-Ti	−0.155 ± 0.007	4.6 ± 0.2
Ni-P-650 °C	−0.096 ± 0.004	6.0 ± 0.3
Ni-P-Ti-650 °C	−0.139 ± 0.003	1.8 ± 0.2

3.4. Dynamic Corrosion in the Presence of Abrasive Particles

To study the influence of abrasive particles on the corrosion behavior of coatings, potentiodynamic polarization tests were conducted in a 3.5 wt % NaCl solution in the presence of abrasive particles under a flowing condition (900 rpm) up to 2 h. Representative potentiodynamic polarization curves of AISI 1018 steel substrate, as-deposited coatings, and annealed coatings in the presence of abrasive particles under a flowing condition (900 rpm) are shown in Figure 4. It is observed that as-deposited and annealed coatings exhibit much higher corrosion potential than AISI 1018 steel substrate, which suggests the lower corrosion tendency of the coatings in the presence of abrasive particles under a flowing condition.

Using Tafel extrapolation, the corrosion potential (E_{corr}) and corrosion current density (i_{corr}) were extracted from potentiodynamic polarization curves. Corrosion characteristics of AISI 1018 steel substrate, as-deposited coatings, and annealed coatings in the presence of abrasive particles under a flowing condition (900 rpm) are given in Table 3. The dynamic corrosion currents in the presence of abrasive particles are much higher than the dynamic corrosion currents in the absence of abrasive particles (Table 2). In the presence of abrasive particles under a flowing condition, the dynamic corrosion current of the as-deposited Ni-P coating is only 54% of that of AISI 1018 steel due to its high hardness and corrosion resistance. Compared to the as-deposited Ni-P coating, the as-deposited Ni-P-Ti coating exhibits lower dynamic corrosion current due to its higher toughness to resist impacts. Similarly, the dynamic corrosion current of annealed Ni-P-Ti is lower than that of the annealed Ni-P coating. In addition, the annealed Ni-P coating shows a lower dynamic

corrosion current compared to the as-deposited Ni-P coating due to its improved toughness after crystallization to withstand impacts. The annealed Ni-P-Ti coating also shows a lower dynamic corrosion current than the as-deposited Ni-P-Ti coating due to the formation of NiTi phase after annealing. NiTi alloy is known for its high impact and corrosion resistance [28,29]. Therefore, the presence of NiTi in other composites can improve their impact and corrosion resistance, as confirmed by other studies [30,31]. The lowest dynamic corrosion current is achieved on an annealed Ni-P-Ti coating among all the tested samples, which is only 25% of the as-deposited Ni-P coating.

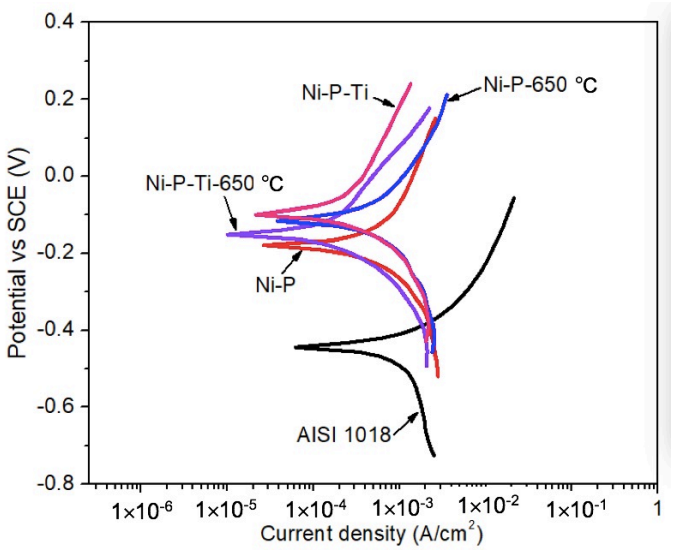

Figure 4. Representative potentiodynamic polarization curves of AISI 1018 steel substrate, as-deposited coatings, and annealed coatings in the presence of abrasive particles under a flowing condition (900 rpm).

Table 3. Corrosion characteristics of AISI 1018 steel substrate, as-deposited coatings, and annealed coatings derived from polarization curves in the presence of abrasive particles under a flowing condition (900 rpm).

Samples	E_{corr} (V)	i_{corr} (μA/cm^2)
AISI 1018 steel	-0.446 ± 0.005	801 ± 7
Ni-P	-0.167 ± 0.004	434 ± 5
Ni-P-Ti	-0.115 ± 0.005	132 ± 3
Ni-P-650 °C	-0.136 ± 0.003	220 ± 5
Ni-P-Ti-650 °C	-0.139 ± 0.002	113 ± 3

3.5. Comparison between Static and Dynamic Corrosion

Corrosion is sensitive to environment; materials in different environments may have different performance. To investigate the corrosion behavior of as-deposited and annealed coatings, corrosion tests were carried out under different conditions, including static corrosion, dynamic corrosion in the absence of abrasive particles, and dynamic corrosion in the presence of abrasive particles using potentiodynamic polarization in 3.5 wt % sodium chloride solutions. The corrosion current density (i_{corr}) and corrosion potential (E_{corr}) were extracted from polarization curves using Tafel extrapolation. The corrosion rate (CR: mm/year) was calculated according to ASTM G102 [31]:

$$CR = \frac{i_{corr} \times EW}{D} \times 3.27 \times 10^{-3} \quad (1)$$

where EW is the equivalent atomic weight, D is the density of the coatings (g/cm^3), and i_{corr} is expressed as μA/cm^2.

The corrosion rates of as-deposited and annealed Ni-P and Ni-P-Ti coatings under different conditions are given in Table 4. The static corrosion resistance of annealed coatings is slightly lower than that of as-deposited coatings (Table 4). For example, the average static corrosion rate of annealed Ni-P-Ti coating is 3.60×10^{-2} mm/year, which is slightly higher than that of as-deposited Ni-P-Ti coating (2.90×10^{-2} mm/year). This is mainly due to the presence of grain boundaries as a result of crystallization after annealing, which are vulnerable sites for corrosion [32]. However, the static corrosion rate of the annealed Ni-P-Ti coating (3.60×10^{-2} mm/year) is only 39% that of the as-deposited Ni-P coating (9.02×10^{-2} mm/year). This suggests that the annealed Ni-P-Ti coating still has much higher static corrosion resistance than the as-deposited Ni-P coating.

Table 4. Comparison between static and dynamic corrosion rates.

Coatings	Static Corrosion Rate (mm/Year)	Dynamic Corrosion Rate (mm/Year, in the Absence of Abrasive Particles, under Flowing Condition 900 rpm)	Dynamic Corrosion (mm/Year, in the Presence of Abrasive Particles, under Flowing Condition 900 rpm)
Ni-P	$9.02 \pm 0.16 \times 10^{-2}$	2.84 ± 0.05	49.7 ± 0.5
Ni-P-Ti	$2.90 \pm 0.14 \times 10^{-2}$	0.43 ± 0.03	12.8 ± 0.3
Ni-P-650 °C	$1.10 \pm 0.13 \times 10^{-1}$	0.61 ± 0.07	18.7 ± 0.4
Ni-P-Ti-650 °C	$3.60 \pm 0.15 \times 10^{-2}$	0.14 ± 0.05	10.1 ± 0.2

Compared to static corrosion rates, the dynamic corrosion rates in the absence of abrasive particles under flowing condition (900 rpm) are one to two orders of magnitude higher (Table 4). This is mainly because of the flowing condition. The flowing sodium chloride solution causes cavitation on the coating surface, which accelerates corrosion rates. Unlike static corrosion, it is interesting to note that the dynamic corrosion rate of annealed coatings is lower than that of as-deposited coatings (e.g., annealed Ni-P-Ti coating: 0.14 mm/year vs. as-deposited Ni-P-Ti coating: 0.43 mm/year) due to their improved toughness after annealing. In addition, in the absence of abrasive particles, the lowest dynamic corrosion rate is reached on annealed Ni-P-Ti coatings among all the tested coatings, which is only 5% that of the as-deposited Ni-P coating.

Compared to dynamic corrosion rates in the absence of abrasive particles, dynamic corrosion rates in the presence of abrasive particles are approximately one order of magnitude higher (Table 4). In the absence of erosive particles, the passive oxide film (NiO) prevents the coating from further corrosion [4]. On the other hand, in the presence of erosive particles, the passive film is removed by abrasive particles, which exposes more vulnerable fresh surface to the corrosive solution [3]. In addition, the high strained sites on the coating surface due to the impacts of abrasive particles are susceptible to corrosion, since they are more anodic than the unstrained sites [5]. These factors result in higher dynamic corrosion rates in the presence of abrasive particles compared to the dynamic corrosion rates in the absence of abrasive particles. Unlike the static corrosion, annealed coatings have higher dynamic corrosion resistance than as-deposited coatings in the presence of abrasive particles due to their increased toughness (e.g., annealed Ni-P-Ti coating: 10.1 mm/year vs. as-deposited Ni-P-Ti coating: 12.8 mm/year). The lowest dynamic corrosion rate in the presence of abrasive particles is achieved on the annealed Ni-P-Ti coating among all the tested coatings, which is only 20% that of the as-deposited Ni-P coating.

3.6. Corrosion Mechanisms

To investigate the corrosion mechanisms of different coatings, the coatings before and after static and dynamic corrosion were examined under SEM. Representative SEM micrographs of as-deposited and annealed Ni-P coatings before and after 2 h static and dynamic corrosion tests are shown in Figure 5. Nodular structure and pores are observed on as-deposited and annealed Ni-P coatings (Figure 5a,b). The formation of pores in the

as-deposited and annealed Ni-P coating is due to the evolution of hydrogen during the oxidation of $NaPO_2H_2$ in the electroless plating process [33]. These pores are the vulnerable sites for pitting corrosion, as observed in Figure 5c,d. During the static corrosion process, the corrosive solution penetrates into a pore, causing Ni dissolution. The dissolution depletes oxygen in the pore due to the stagnancy of the corrosive solution. As a result, the surface areas around the pore act as a cathode, while the pore itself acts as an anode, which accelerates pitting corrosion due to a large cathode to anode area ratio.

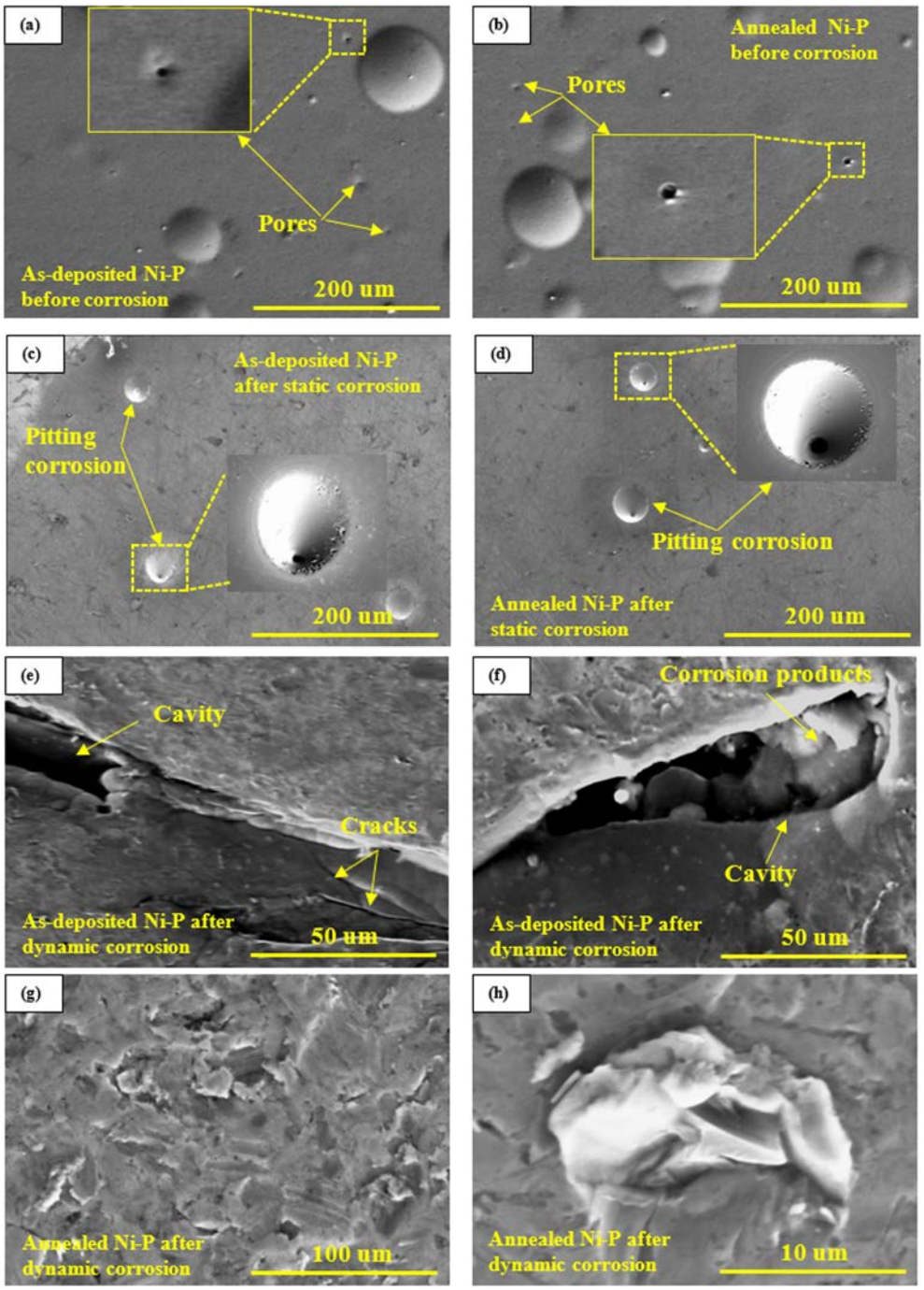

Figure 5. Representative SEM micrographs of (**a**) as-deposited Ni-P coating before corrosion tests, (**b**) annealed Ni-P coating before corrosion tests, (**c**) as-deposited Ni-P coating after static corrosion test, (**d**) annealed Ni-P coating after static corrosion test, (**e**,**f**) as-deposited Ni-P coating after dynamic corrosion test in the presence of abrasive particles, (**g**,**h**) annealed Ni-P coating after dynamic corrosion test in the presence of abrasive particles.

Cracks and cavities are observed on the as-deposited Ni-P coating after dynamic corrosion in the presence of abrasive particles under a flowing condition (Figure 5e,f). This is due to the low toughness of the as-deposited Ni-P coating, as confirmed in our previous studies [13,23]. The impacts of abrasive particles cause cracking on as-deposited Ni-P coating; then, the cracks propagate into the coating and connect to each other, resulting in coating delamination. Then, the debris of coating delamination was removed by abrasive particles in the subsequent impacts and by the flowing solution. This results in cavities which are favorable sites for localization corrosion (i.e., erosion-enhanced corrosion). Corrosion products are observed in a cavity (Figure 5f). On the other hand, no cracking and fracture are observed on the annealed Ni-P coating due to its improved toughness after annealing [34]; a highly strained surface is observed on the annealed Ni-P coating (Figure 5g,h). The highly strained surface is more susceptible to corrosion due to its high energy. Here, erosion accelerates corrosion by producing a strained surface that is vulnerable to corrosion. Corrosion in this case may be classified as uniform corrosion.

Representative SEM micrographs of as-deposited and annealed Ni-P-Ti coatings before and after 2 h static and dynamic corrosion tests are shown in Figure 6. Compared to as-deposited and annealed Ni-P coatings (Figure 5a,b), no pores are observed on as-deposited and annealed Ni-P-Ti coatings (Figure 6a,b). This is mainly because Ti nanoparticles can occupy and fill the pores in the Ni-P matrix. In addition, the presence of Ti particles seems to prevent the growth of Ni-P nodules, resulting in a denser and finer surface [35]. After static corrosion, no pits are observed on as-deposited and annealed Ni-P-Ti coatings (Figure 6c,d). A uniform, dense, and smooth surface is observed on the as-deposited and annealed Ni-P-Ti coatings (Figure 6c,d), which indicates the high static corrosion resistance of as-deposited and annealed Ni-P-Ti coatings. After dynamic corrosion in the presence of abrasive particles under a flowing condition, a strained surface is developed on the as-deposited Ni-P-Ti coatings (Figure 6e,f). However, compared to the annealed Ni-P coating (Figure 5g,h)), surface damage on the as-deposited Ni-P-Ti coating is less severe (Figure 6e,f) due to its higher hardness. Among all the tested coatings, the annealed Ni-P coating has the lowest hardness, whereas the annealed Ni-P-Ti coating has the highest hardness, as confirmed in our previous study [13]. In addition, spallation is observed on the as-deposited Ni-P-Ti coating. In some cases, the repeated impacts cause microcracks on the coating surface, leading to the corrosive solution penetrating the subsurface layer through the microcracks and corroding the subsurface layer. Subsequently, the unsupported top layer is removed by the following impacts, which results in spallation on the as-deposited Ni-P-Ti coating.

On the other hand, unlike the annealed Ni-P coating (Figure 5g,h) and as-deposited Ni-P-Ti coating (Figure 6e,f), no severe surface damage and coating spallation is observed on the annealed Ni-P-Ti coating (Figure 6g,h). A smooth and uniform surface with shallow micro-size scratch scars and indents are observed on the annealed Ni-P-Ti coating (Figure 6g,h). This highlights the high dynamic corrosion resistance of the annealed Ni-P-Ti coating due to the formation of a superelastic NiTi phase within the coating after annealing. During the impact process, the austenite phase within the NiTi particles transforms to a detwinned martensite phase accompanied by large surface deformation, which absorbs the impact energy of erosive particles [34]. The impact energy is absorbed and stored in the detwinned martensite phase. When erosive particles leave the surface, the detwinned martensite phase transforms back to austenite phase with deformation recovery [34]. This stress-induced phase transformation significantly improves the toughness of the annealed Ni-P-Ti coating [26,34] and results in an unstrained coating surface, which leads to the improved dynamic corrosion resistance of annealed Ni-P-Ti coating in the presence of abrasive particles under flowing condition.

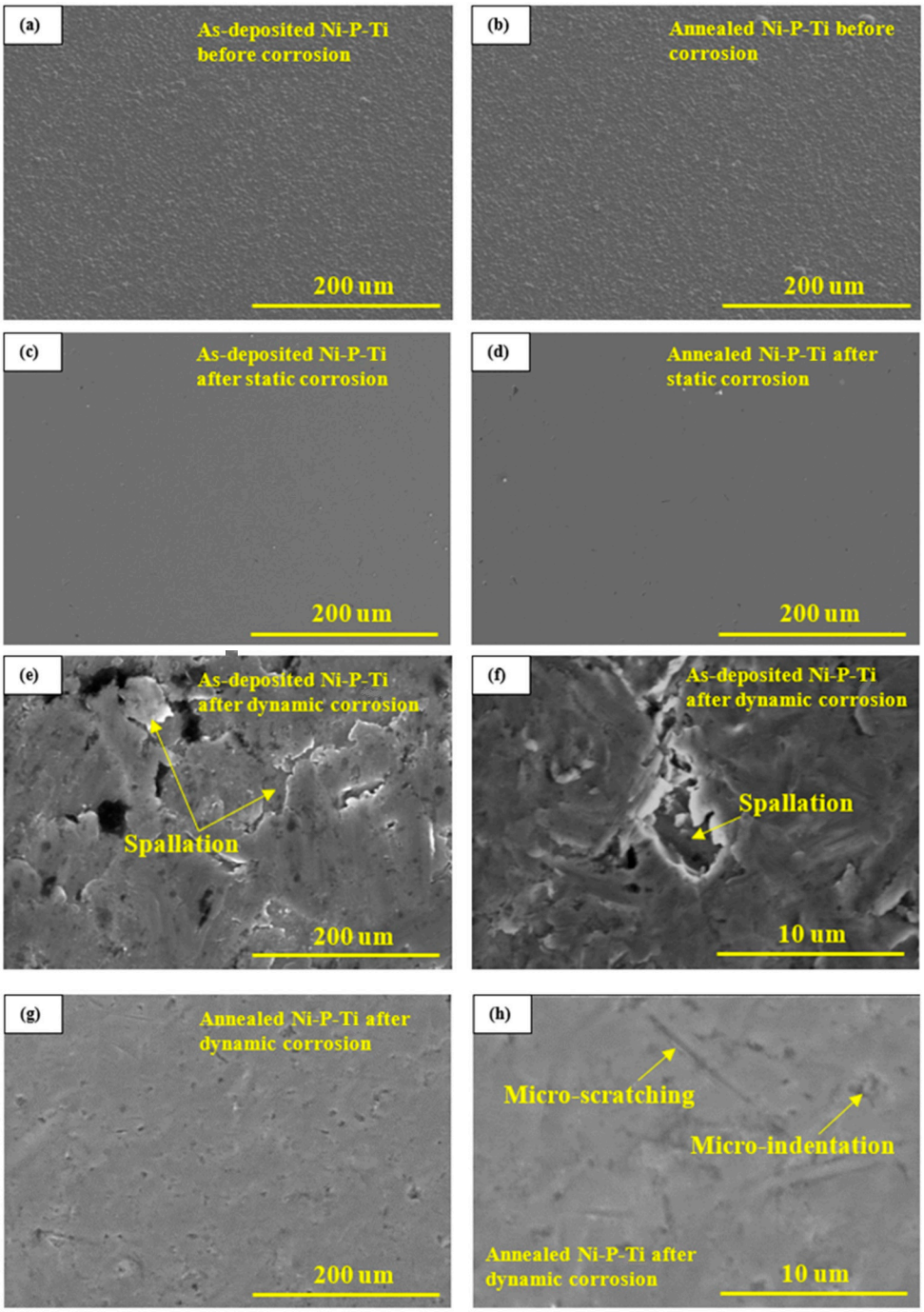

Figure 6. Representative SEM micrographs of (**a**) as-deposited Ni-P-Ti coating before corrosion tests, (**b**) annealed Ni-P-Ti coating before corrosion tests, (**c**) as-deposited Ni-P-Ti coating after static corrosion test, (**d**) annealed Ni-P-Ti coating after static corrosion test, (**e**,**f**) as-deposited Ni-P-Ti coating after dynamic corrosion test in the presence of abrasive particles, (**g**,**h**) annealed Ni-P-Ti coating after dynamic corrosion test in the presence of abrasive particles.

To further investigate the corrosion behavior of different coatings, the porosity density (P.D.) of different coatings under static and dynamic corrosion conditions were calculated using the following equation [36]:

$$\text{P.D.} = \frac{R_s}{R_c} \times 10^{-\frac{\Delta E}{\beta_\alpha}} \quad (2)$$

where R_s represents the polarization resistance of steel substrate; ΔE represents the potential difference between the steel substrate and the coating; R_c represents the polarization resistance of the coating; β_α represents the slope of anodic Tafel extrapolation of the steel substrate.

The porosity density (P.D.) of different coatings is given in Table 5. The porosity density value of the as-deposited Ni-P coating is 2.64%, which is consistent with the value (2.4%) obtained in Mazaheri et al.'s study [35]. Compared to as-deposited and annealed Ni-P coatings, the porosity density values of as-deposited and annealed Ni-P-Ti coatings are lower due to the presence of Ti nanoparticles that occupy and fill the nano and micro-size pores in the Ni-P matrix. This leads to a dense surface of Ni-P-Ti coatings, which is verified in Figure 6a,b. The porosity density values of the coatings under dynamic corrosion conditions without abrasive particles are higher than those under static corrosion due to the cavitation erosion caused by flowing solution. Among three different corrosion conditions, the highest porosity density values are observed under dynamic corrosion in the presence of abrasive particles. This is due to the erosion, which increased corrosion by the impacts of abrasive particles. For the dynamic corrosion conditions (with and without abrasive particles), the highest dynamic corrosion resistance is achieved on an annealed Ni-P-Ti coating (Ni-P-Ti-650 °C coating) that exhibits the lowest porosity density value among all the tested coatings. The porosity density results are in good agreement with the corrosion rates results.

Table 5. Porosity density (P.D.) of different coatings under static and dynamic corrosion conditions.

Coatings	P.D. (%) Static Corrosion	P.D. (%) Dynamic Corrosion (in the Absence of Abrasive Particles, under Flowing Condition 900 rpm)	P.D. (%) Dynamic Corrosion (in the Presence of Abrasive Particles, under Flowing Condition 900 rpm)
Ni-P	2.64 ± 0.16	11.72 ± 0.15	29.01 ± 1.91
Ni-P-Ti	0.18 ± 0.03	4.52 ± 0.05	11.75 ± 0.32
Ni-P-650 °C	2.72 ± 0.13	6.74 ± 0.07	14.86 ± 0.43
Ni-P-Ti-650 °C	0.20 ± 0.02	3.47 ± 0.05	7.18 ± 0.22

To evaluate constituents' changes on coatings before and after 2 h dynamic corrosion in the presence of abrasive particles, EDS analysis was employed. Figures 7 and 8 show the surface SEM micrographs, corresponding EDS maps, and spectra of annealed Ni-P-Ti coatings before and after dynamic corrosion, respectively. From Figure 7, it is observed that the Ti element is uniformly distributed along the surface of the coating. A very small amount (0.78 wt %) of oxygen is detected on the surface (Figure 7f). After dynamic corrosion in the presence of abrasive particles (Figure 8), there is no obvious change on Ti element distribution compared to before dynamic corrosion (Figure 7). Although oxygen content increases to 1.35 wt % due to the dynamic corrosion (Figure 8f), the oxygen content is still very low. This low oxygen content indicates the high dynamic corrosion resistance of the annealed Ni-P-Ti coating. Except for the oxygen content, there is no significant change on other elements content (Ni, P, and Ti) before and after dynamic corrosion.

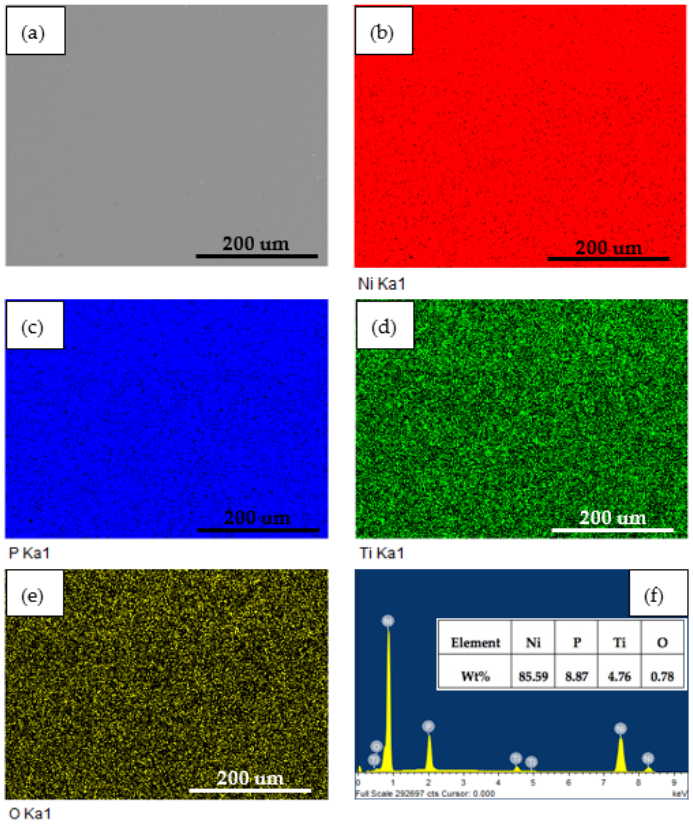

Figure 7. (**a**) Surface SEM micrograph, (**b**–**e**) corresponding EDS elemental maps, and (**f**) EDS spectrum of annealed Ni-P-Ti coating before dynamic corrosion.

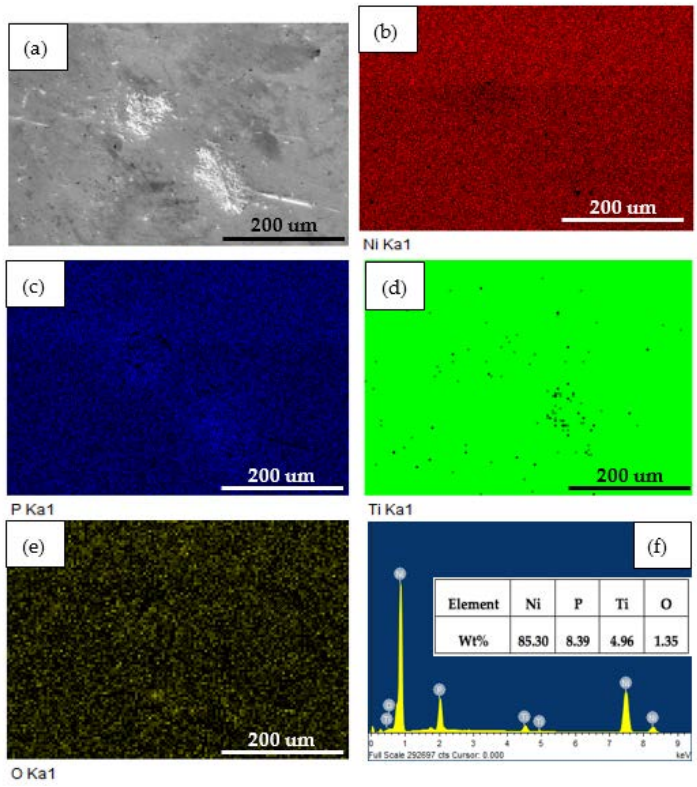

Figure 8. (**a**) Surface SEM micrograph, (**b**–**e**) corresponding EDS elemental maps, and (**f**) EDS spectrum of annealed Ni-P-Ti coating after dynamic corrosion in the presence of abrasive particles.

4. Conclusions

Ni-P-NiTi composite coatings were successfully prepared on AISI 1018 steel by incorporating Ti nanoparticles into the Ni-P matrix followed by the annealing of electroless Ni-P-Ti coatings. Static corrosion, dynamic corrosion in the absence of abrasive particles under a flowing condition, and dynamic corrosion performance in the presence of abrasive particles under a flowing condition of as-deposited and annealed Ni-P and Ni-P-Ti coatings were studied. The effect of the formation of the superelastic NiTi phase on the static corrosion and dynamic corrosion performance was investigated. It was found that the annealed Ni-P-Ti coating (i.e., Ni-P-NiTi coating) exhibited much higher static corrosion resistance than the as-deposited Ni-P coating. Among all the tested samples, the annealed Ni-P-Ti coating (i.e., Ni-P-NiTi coating) has the highest dynamic corrosion resistance in the absence and presence of abrasive particles under flowing conditions. The dynamic corrosion resistance of the annealed Ni-P-Ti coating (i.e., Ni-P-NiTi coating) is 19 times higher than that of the as-deposited Ni-P coating in the absence of abrasive particles under a flowing condition. The dynamic corrosion resistance of the annealed Ni-P-Ti coating (i.e., Ni-P-NiTi coating) is four times higher than that of the as-deposited Ni-P coating in the presence of abrasive particles under a flowing condition. The formation of a superelastic NiTi phase substantially improved the static and dynamic corrosion performance of the electroless Ni-P coating.

Author Contributions: Conceptualization, Z.F. and Z.L.; methodology, Z.F. and Z.L.; formal analysis, Z.L.; investigation, Z.L.; resources, Z.L.; data curation, Z.L.; writing—original draft preparation, Z.L.; writing—review and editing, Z.F.; supervision, Z.F.; Both authors have read and agreed to the published version of the manuscript.

Funding: This research was funded by Natural Scientific and Engineering Research Council of Canada, grant number RGPIN 327449 and The APC was funded by Natural Scientific and Engineering Research Council of Canada.

Institutional Review Board Statement: Not applicable.

Informed Consent Statement: Not applicable.

Data Availability Statement: Not available.

Conflicts of Interest: The authors declare no conflict of interest.

References

1. Gandy, D. *Carbon Steel Handbook*; Electri Power Research Institute: Palo Alto, CA, USA, 2007; pp. 1–172.
2. MacLean, M.; Farhat, Z.; Jarjoura, G.; Fayyad, E.; Abdullah, A.; Hassan, M. Fabrication and investigation of the scratch and indentation behaviour of new generation Ni-P-nano-NiTi composite coating for oil and gas pipelines. *Wear* **2019**, *426*, 265–276. [CrossRef]
3. Islam, M.A.; Farhat, Z. The synergistic effect between erosion and corrosion of API pipeline in CO_2 and saline medium. *Tribol. Int.* **2013**, *68*, 26–34. [CrossRef]
4. Islam, M.A.; Farhat, Z. Erosion-corrosion mechanism and comparison of erosion-corrosion performance of API steels. *Wear* **2017**, *376–377*, 533–541. [CrossRef]
5. Islam, M.A.; Farhat, Z.; Ahmed, E.M.; Alfantazi, A.M. Erosion enhanced corrosion and corrosion enhanced erosion of API X-70 pipeline steel. *Wear* **2013**, *302*, 1592–1601. [CrossRef]
6. Taubkin, I.; Sukchov, A.V.; Rudakova, T. Analysis of the behavior of a protective polymer coating for gas pipelines under the action of applied heat. *Int. Polym. Sci. Technol.* **2004**, *32*, 22–32. [CrossRef]
7. Bayram, T.C.; Orbey, N.; Adhikari, R.Y.; Tuominen, M. FP-based formulations as protective coatings in oil/gas pipelines. *Prog. Org. Coat.* **2015**, *88*, 54–63. [CrossRef]
8. Vojtěch, D.; Novák, M.; Zelinková, M.; Novák, P.; Michalcová, A.; Fabián, T. Structural evolution of electroless Ni–P coating on Al–12wt.% Si alloy during heat treatment at high temperatures. *Appl. Surf. Sci.* **2009**, *255*, 3745–3751. [CrossRef]
9. Lee, C.K. Structure, electrochemical and wear-corrosion properties of electroless nickel–phosphorus deposition on CFRP composites. *Mater.Chem. Phys.* **2009**, *114*, 125–133. [CrossRef]
10. Xu, X.; Miao, J.; Bai, Z.; Feng, Y.; Ma, Q.; Zhao, W. The corrosion behavior of electroless Ni–P coating in Cl^-/H_2S environment. *Appl. Surf. Sci.* **2012**, *258*, 8802–8806.

11. Wang, C.; Farhat, Z.; Jarjoura, G.; Hassan, M.K.; Abdullah, A.M. Indentation and erosion behavior of electroless Ni-P coating on pipeline steel. *Wear* **2017**, *376–377*, 1630–1639. [CrossRef]
12. Farhat, Z.; Jarjoura, G.; Shahirnia, M. Dent Resistance and Effect of Indentation Loading Rate on Superelastic TiNi Alloy. *Metall. Mater. Trans. A* **2013**, *44*, 3544–3551. [CrossRef]
13. Li, Z.; Farhat, Z. Hertzian Indentation Behavior of Electroless Ni-P-Ti Composite Coatings. *Metall. Mater. Trans. A* **2020**, *51*, 3674–3691. [CrossRef]
14. Li, Z.; Farhat, Z.; Jarjoura, G.; Fayyad, E.; Abdullah, A.; Hassan, M. Investigation of the mechanical behavior of electroless Ni-P-Ti composite coatings. *J. Eng. Mater. Technol.* **2020**, *142*, 1–12. [CrossRef]
15. Sharifalhoseini, Z.; Entezari, M.H.; Davoodi, A.; Shahidi, M. Access to nanocrystalline, uniform, and fine-grained Ni-P coating with improved anticorrosive action through the growth of ZnO nanostructures before the plating process. *Corros. Sci.* **2020**, *172*, 108743. [CrossRef]
16. Ghavidel, N.; Allahkaram, S.R.; Naderi, R.; Barzegar, M.; Bakhshandeh, H. Corrosion and wear behavior of an electroless Ni-P/nano-SiC coating on AZ31 Mg alloy obtained through environmentally-friendly conversion coating. *Surf. Coat. Technol.* **2020**, *382*, 125156. [CrossRef]
17. Li, Y.; Zhang, K.; Zhang, M.; Zhang, Y.; Wu, T.; Zhao, H. Effect of current density on properties of sol-enhanced Ni–P– Al_2O_3 composite coating. *Int. J. Electrochem. Sci.* **2020**, *15*, 2752–2765. [CrossRef]
18. Dhakal, D.R.; Gyawali, G.; Kshetri, Y.K.; Choi, J.H.; Lee, S.W. Microstructural and electrochemical corrosion properties of electroless Ni-P-TaC composite coating. *Surf. Coat. Technol.* **2020**, *381*, 125135. [CrossRef]
19. Xie, J.; Alpas, A.T.; Northwood, D.O. Mechano-electrochemical effect between erosion and corrosion. *J. Mater. Sci.* **2003**, *38*, 4849–4856. [CrossRef]
20. Tian, X.; Zhang, H. Failure criterion of buried pipelines with dent and scratch defects. *Eng. Fail. Anal.* **2017**, *80*, 278–289. [CrossRef]
21. Sun, C.; Li, J.; Fattahpour, V.; Roostaei, M.; Mahmoudi, M.; Zeng, H.; Luo, J.-L. Insights into the erosion-enhanced corrosion on electroless Ni–P coating from single particle impingement. *Corros. Sci.* **2020**, *166*, 108422–108434. [CrossRef]
22. Li, Z.; Farhat, Z. Effects of Ti content and annealing temperatures on fracture toughness and scratch resistance of electroless Ni-P-Ti coatings. *J. Mater. Eng. Perform.* **2020**, *29*, 5807–5821. [CrossRef]
23. Li, Z.; Islam, M.A.; Farhat, Z. Investigation of Erosion-Corrosion Resistance of Electroless Ni-P-Ti Composite Coatings. *J. Bio-Tribo-Corros.* **2020**, *6*, 1–17. [CrossRef]
24. Islam, M.A.; Jiang, J.; Xie, Y.; Fiala, P. Investigation of erosion-corrosion behavior of (WTi)C based weld overlays. *Wear* **2017**, *390–391*, 155–165. [CrossRef]
25. Li, Z.; Farhat, Z.; Jarjoura, G.; Fayyad, E.; Abdullah, A.; Hassan, M. Synthesis and characterization of scratch resistant Ni-P-Ti based composite coating. *Tribol. Trans.* **2019**, *62*, 880–896. [CrossRef]
26. Li, Z.; Farhat, Z. Microstructure development and nanoindentation behavior of annealed Ni-P-Ti coatings. *Surf. Eng.* **2021**, *37*, 1–15. [CrossRef]
27. Diegle, R.B.; Sorensen, N.R.; Clayton, C.R.; Helfand, M.A.; Yu, Y.C. An XPS investigation into the passivity of an amorphous Ni-20P. *J. Electrochem. Soc.* **1988**, *135*, 1085–1092. [CrossRef]
28. Shi, Z.; Wang, J.; Wang, Z.; Qiao, Y.; Xiong, T.; Zheng, Y. Cavitation erosion and jet impingement erosion behavior of the NiTi coating produced by air plasma spraying. *Coatings* **2018**, *8*, 346–357. [CrossRef]
29. Kosec, T.; Močnik, P.; Mezeg, U.; Legat, A.; Ovsenik, M.; Jenko, M.; Grant, J.T.; Primožič, J. Tribocorrosive study of new and in vivo exposed nickel titanium and stainless steel orthodontic archwires. *Coatings* **2020**, *10*, 230–242. [CrossRef]
30. Angioni, S.L.; Meo, M.; Foreman, A. Impact damage resistance and damage suppression properties of shape memory alloys in hybrid composites-a review. *Smart Mater. Struct.* **2011**, *20*, 013001. [CrossRef]
31. Verdian, M.M.; Raeissi, K.; Salehi, M.; Sabooni, S. Characterization and corrosion behavior of NiTi–Ti_2Ni–Ni_3Ti multiphase intermetallics produced by vacuum sintering. *Vacuum* **2011**, *86*, 91–95. [CrossRef]
32. Ciubotariu, A.-C.; Benea, L.; Lakatos-Varsanyi, M.; Dragan, V. Electrochemical impedance spectroscopy and corrosion behaviour of Al_2O_3-Ni nano composite coatings. *Electrochim. Acta.* **2008**, *53*, 4557–4563. [CrossRef]
33. Lin, C.; Dadvand, N.; Farhat, Z.; Kipouros, G. Electroless nickel phosphorous plating on carbon steel. *Mater. Sci. Technol.* **2013**, *3*, 2224–2237.
34. Li, Z.; Farhat, Z.; Islam, M.A. Investigation of Single-Particle Erosion Behavior of Electroless Ni-P-Ti Composite Coatings. *J. Mater. Eng. Perform.* **2020**, *29*, 1671–1683. [CrossRef]
35. Mazaheri, H.; Allahkaram, S.R. Deposition, characterization and electrochemical evaluation of Ni–P–nano diamond composite coatings. *Appl. Surf. Sci.* **2012**, *258*, 4574–4580. [CrossRef]
36. Creus, J.; Mazille, H.; Idrissi, H. Porosity evaluation of protective coatings onto steel through electrochemical technique. *Surf. Coat. Technol.* **2000**, *130*, 224–232. [CrossRef]